Available online at www.sciencedirect.com
ScienceDirect
International Journal of Heat and Fluid Flow 28 (2007) 1144–1156
International Journal of HEAT AND FLUID FLOW
www.elsevier.com/locate/ijhff

Numerical simulation and theoretical analysis of thermal boundary characteristics of convection heat transfer in porous media

Pei-Xue Jiang *, Xiao-Chen Lu

Key Laboratory for Thermal Science and Power Engineering, Department of Thermal Engineering, Tsinghua University, Beijing 100084, China

Received 24 May 2005; received in revised form 6 July 2006; accepted 9 November 2006
Available online 6 February 2007

Abstract

The thermal boundary characteristics at the contact interface between a porous media and an impermeable wall subject to a constant heat flux on its upper surface with and without consideration of the thermal contact resistance were investigated using a particle-level numerical simulation of single phase fluid flow and convection heat transfer in porous media. The numerical simulations assumed an ideal packed bed (simple cubic structure) formed by uniform diameter particles with small contact areas and a zero- or finite-thickness wall subject to a constant heat flux at the surface which mirrors the experimental setup. The numerical simulations showed that the temperature distribution at the contact interface is non-uniform for the porous media with a zero-thickness impermeable wall, and in the porous media with a finite-thickness impermeable wall with a thermal contact resistance between the particles and the plate (such as with a non-sintered porous media) with a constant heat flux on the outer surface, while the heat flux distribution at the contact interface is quite uniform for these cases. However, in the porous media with a finite-thickness impermeable wall without a thermal contact resistance between the particles and the plate (such as with a sintered porous media) with a constant heat flux on the outer surface, the heat flux distribution at the contact interface is very non-uniform, while the temperature distribution at the contact interface is quite uniform. Numerical simulations of the thermal boundary characteristics of the convection heat transfer in the porous media were used to investigate the applicability of various boundary conditions for the energy equations with and without a thermal contact resistance between the particles and the plate wall.

Keywords: Thermal boundary characteristics; Heat transfer; Porous media; Particles; Thermal contact resistance

1. Introduction

Forced convection heat transfer in porous media has many important applications, such as geothermal energy extraction, catalytic and chemical particle beds, petroleum processing, transpiration cooling, solid matrix heat exchangers, packed-bed regenerators, and heat transfer enhancement. Therefore, fluid flow and convective heat transfer in porous media have received much attention for many years.

There have been numerous theoretical and numerical investigations of convection heat transfer in fluid-saturated porous media. The numerical investigations of convection heat transfer in porous media have used two different models for the energy equation: the local thermal equilibrium model and the local thermal non-equilibrium model. The local thermal equilibrium model assumes that the solid-phase temperature is equal to the fluid temperature, i.e., local thermal equilibrium between the fluid and solid phases at every location in the porous media. This model simplifies the theoretical and numerical investigations, but the assumption of local thermal equilibrium between the fluid and solid phases is inadequate for many situations. In recent years the local thermal non-equilibrium model has been used more frequently in the energy equation in theoretical and numerical research on convection heat transfer in porous media (Amiri and Vafai, 1994;

* Corresponding author. Tel.: +86 10 62772661; fax: +86 10 62770209.
E-mail address: jiangpx@tsinghua.edu.cn (P.-X. Jiang).

0142-727X/$ - see front matter © 2006 Elsevier Inc. All rights reserved.
doi:10.1016/j.ijheatfluidflow.2006.11.009

Nomenclature

a	central distance between two adjacent particles (m)
c_p	specific heat (J/kg K)
d_p	particle diameter (m)
F	inertia coefficient
h	convection heat transfer coefficient (W/m^2 K)
K	porous medium permeability (m^2)
p	pressure (Pa)
q	heat transfer (W/m^2)
T	temperature (K)
u, v, w	velocity (m/s)
u_0	inlet fluid velocity (m/s)
x, y, z	coordinates (m)

Greek symbols

δ	wall thickness (mm)
ε	porosity
λ	thermal conductivity (W/m K)
μ	absolute viscosity (N s/m^2)
ρ	fluid density (kg/m^3)

Subscripts

0	inlet
C	correlation results
f	fluid
m	mean
N	numerical results
o	out
p	particle
s	solid
w	wall

Jiang and Ren, 2001; Jiang et al., 1996, 2002, 2004a; Hsieh and Lu, 2000; Alazmi and Vafai, 2002) to more accurately model the convection heat transfer processes in porous media.

With the thermal non-equilibrium model, the treatment of the boundary conditions for the energy equation significantly affects the simulation results. A number of papers have analyzed this problem, e.g. Amiri et al. (1995), Quintard (1998), Peterson and Chang (1998), Martin et al. (1998), Lee and Vafai (1999), Jiang and Ren (2001), Jiang et al., 2002, 2004a,b and Alazmi and Vafai (2002). For the constant heat flux boundary condition, there are several different methods to treat the energy equation boundary conditions. The main differences among them are whether the fluid temperature is equal to the solid phase temperature at the boundary surface and how to determine the heat flux transferred through the solid phase and the fluid. Alazmi and Vafai (2002) analyzed 8 different forms of the constant wall heat flux boundary conditions in the absence of local thermal equilibrium conditions in porous media. They found that different boundary conditions may lead to substantially different results. At the same time, they pointed out that selecting one model over the others is not an easy issue since previous studies validated each of the two primary models. In addition to that, the mechanics of splitting the heat flux between the two phases is not yet resolved.

Jiang (2001) numerically analyzed the heat transfer boundary characteristics between the surface of a thin plate and a solid particle in contact with each other with convection heat transfer due to water or air in the voids between the solids and a constant heat flux on the outer plate wall. The analysis studied the influence of the thermal contact resistance between the plate wall and the solid particle and the wall thickness on the surface thermal characteristics. The results showed that if the thermal conductivities of the fluid and the solid particle were similar, the temperature and heat flux distributions on the contact surface between the thin plate and the particle and on the convection heat transfer surface of the thin plate were quite uniform, which means that local thermal equilibrium exists for such conditions. If the thermal contact resistance on the wall surface between the solid particles and the plate wall is considered, the solid particle temperature on the contact surface and the fluid temperature on the convection heat transfer surface of the thin plate near the particle are significantly different, while the heat fluxes transferred through the solid particles and the fluid adjacent to the surface are similar. If the thermal contact resistance on the wall surface between the solid particles and the wall is not considered and the plate is relatively thick (e.g. 1–2 mm), the heat fluxes through the solid particles and the fluid near the wall are significantly different, while the temperatures of the solid particles and the fluid near the wall are fairly close, that is $T_{fw} \approx T_{sw}$.

Jiang and Ren (2001) and Jiang et al. (2002, 2004a) investigated the various treatments of the constant heat flux boundary conditions by comparing numerical results with experimental data for forced convection heat transfer of water and air in plate channels filled with non-sintered metallic or non-metallic particles (packed beds) or sintered porous media using a non-thermal equilibrium model. The results showed that for numerical simulations of convection heat transfer in porous media, the boundary condition model significantly influences the numerical results and the proper model must be chosen for the numerical results to agree well with the experimental data. Simulations of convection heat transfer of air or water in non-sintered packed beds using a local thermal non-equilibrium model with the assumption that the heat fluxes transferred by the solid

phase and the fluid from the heat transfer surface were the same with a variable porosity model agreed well with the experimental data. For numerical simulations of convection heat transfer in sintered porous media, the particle temperatures and the fluid temperatures on the wall surface were assumed to be equal. Simulations of convection heat transfer of air or water in sintered bronze porous media using the local thermal non-equilibrium model and the variable porosity model with the wall effect corresponded well to experimental data. The convection heat transfer coefficient in sintered porous media is much higher than that in non-sintered packed beds due to the reduced thermal contact resistance and reduced porosity near the wall in sintered porous media.

Kim and Kim (2001) investigated the heat transfer phenomenon at the interface between a porous medium and an impermeable wall subject to a constant heat flux at the surface. The focus of their paper was to determine which of the thermal boundary conditions is more appropriate for accurately predicting the heat transfer characteristics in a porous channel. They numerically examined the heat transfer at the interface between a microchannel heat sink (assumed to be an ideally organized porous medium) and a finite-thickness substrate. The results clarified that the heat flux distribution at the interface was not uniform for an impermeable wall with finite thickness. Thus, a non-uniform heat flux distribution and a uniform temperature distribution at the interface were determined to be the most physically realistic.

Jiang and Lu (2006) presented particle-level simulations of convection heat transfer in a simple cubic structure formed by particles with the same diameters with small contact areas and a finite-thickness wall subject to a constant heat flux at the surface. The permeability and inertia coefficient were calculated numerically according to the modified Darcy's model. The numerical results were in agreement with well-known correlation results with the calculated local heat transfer coefficients on the plate channel surface agreeing well with the experimental data. The convection heat transfer coefficients between the solid particles and the fluid and the volumetric heat transfer coefficients in the porous media from the simulation increase with increasing mass flow rate and decrease with increasing particle diameter. The particle-level direct simulations of the fluid flow and convection heat transfer in porous media establish a good basis for investigations of the boundary characteristics and internal phenomena controlling the heat transfer in porous media.

The main purpose of the present study is to analyze the thermal boundary characteristics for convection heat transfer in porous media to better understand the heat transfer phenomena and boundary conditions at the interface on the basis of the previous works in Jiang (2001) and Jiang and Lu (2006). Numerical simulations were performed for forced convection heat transfer in a simple cubic (SC) structure formed by uniform diameter particles with small contact areas and a zero- or finite-thickness substrate wall subject to a constant heat flux at the surface. The temperature differences between the fluid and solid phases in the porous media were examined along with the influence of the heated wall with and without a thermal contact resistance between the particles and the wall on the convection heat transfer in the porous media. The proper models for the boundary conditions for the energy equations were identified for flows with and without a thermal contact resistance between the particles and the wall.

2. Physical model, governing equations and numerical method

Particle-level direct numerical simulations of the fluid flow and convection heat transfer in porous media as in Jiang and Lu (2006) were used to numerically investigate the thermal boundary characteristics for convection heat transfer in porous media. A fully numerical solution of the Navier–Stokes equations for the convection heat transfer in a porous media with all the particles is very difficult due to the huge amount of calculation time. Therefore, a limited number of identical particles was used to model the entire porous media with two layers of 5×5 particles as the porous media. The physical model and the coordinate system are shown in Fig. 1. The calculational region included an entrance region with a length of 11 d_p and an exit region with a length of 6 d_p. The packed bed was made of homogeneous, uniform-sized solid particles. The small changes of porosities were obtained by changing the particle sizes and contact areas between the particles. The top surface of the porous media was touching a heated wall whose top surface received a constant heat flux, q_{wo}, while the bottom surface of the channel was thermally insulated. Fluid entered the channel with a uniform velocity, u_0, and constant temperature, T_{f0}. The fluid flow was steady, single-phase and three-dimensional. The heated wall was assumed to have either zero thickness or a finite thickness of 1 mm. For the porous media with the finite thickness heated wall, cases with and without a thermal contact resistance between the particles and the wall were considered.

Table 1 presents the dimensions and porosities of the porous media used in the calculations. ε_w is the wall porosity which is equal to one minus the ratio of the contact area of the particles with the plate to the plate surface area. The contact areas between the particles and the wall surface and the contact areas between particles were assumed to be constant based on the desired porosity. The centerline distance between adjacent particles, a, for actual sintered porous media is a little less than the particle diameter due to the sintering technology.

With non-sintered porous media (packed beds), a thermal contact resistance is known to exist between the particles and between the particles and the wall. These finite contact resistances are due principally to surface roughness effects (Incropera and DeWitt, 1996). The contact resistance may then be viewed as two parallel resistances due to the contact spots and due to the gaps. The contact area

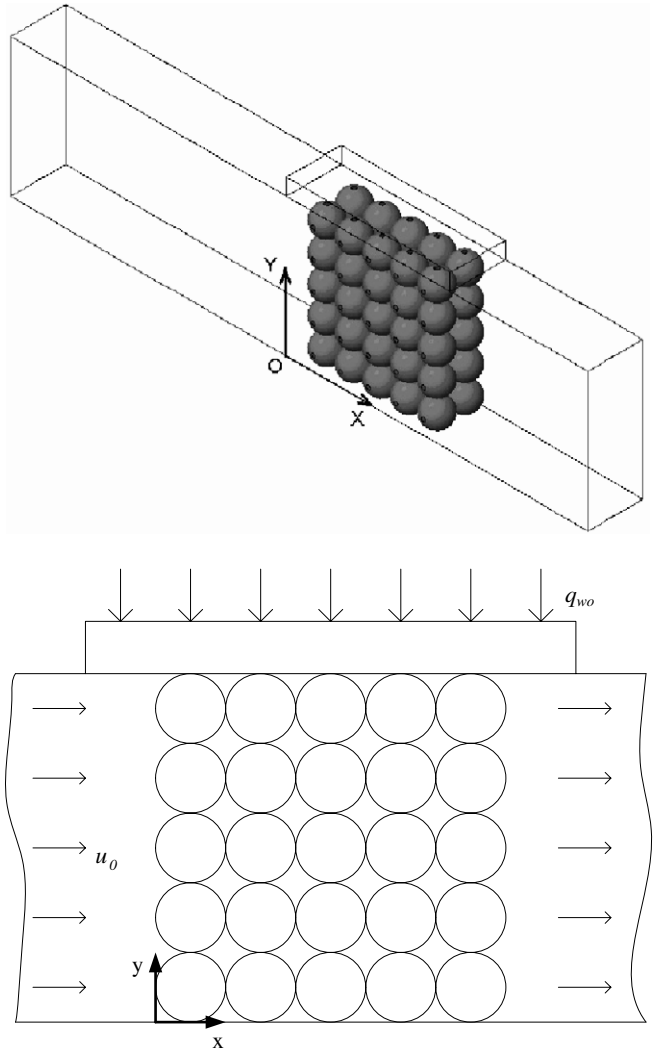

Fig. 1. Schematic diagram of the physical system.

is typically small, and especially for rough surfaces, the major contribution to the resistance is due to the gaps. The surface roughness for metal plates is usually 1–30 μm (Incropera and DeWitt, 1996; Çengel and Turner, 2001). According to Incropera and DeWitt (1996), the thermal contact resistance of an aluminum interface with interfacial air is 2.75×10^{-4} m^2 K/W. However, it is very difficult to accurately determine the thermal contact resistance between particles and the wall in a porous media. For non-sintered porous media, the joint pressure between the particles is usually not large, so the gap between the particles is reasonably assumed to be larger than between two plates at high pressure. Jiang (2001) assumed a 50 μm gap between two adjacent particles for non-sintered porous media with the resulting thermal contact resistance being 2.08×10^{-3} m^{2}K/W which is 7.6 times that between plates. The purpose of the present research is to investigate the thermal boundary characteristics in sintered and non-sintered porous media. The qualitative results are more important, and the value of the thermal contact resistance does not change the qualitative results and conclusions. Therefore, the present paper for non-sintered porous media also used a 50 μm gap between adjacent particles with the results having a thermal contact resistance at the particle interfaces with water of 8.33×10^{-5} m^{2}K/W which is reasonable for thermal contact resistances. As shown in Table 1, the centerline distance between two adjacent particles, a, is larger than the particle diameter for non-sintered porous media.

The calculations assume that the wall is made of copper and the heat flux at the top of the wall is 1×10^5 W/m^2. Water flows through the porous media and removes heat from the porous media and the impermeable wall. The water inlet velocity is 1 mm/s. In the calculations all the physical properties are assumed to be constant. The values of the thermophysical properties used in the calculation are listed in Table 2.

The three-dimensional conjugate heat transfer problem was solved using the CFD software FLUENT 6.1. The Reynolds numbers based on the particle diameters and the inlet velocity for the three geometries listed in Table 1 were 1.6, 1.2 and 0.6. Laminar flow was assumed in the calculations. The SIMPLE algorithm was used to couple the pressure and the velocities with the second order upwind method used for the advection terms in the momentum equations and for the energy equation.

Energy equation for the upper copper plate:

$$\frac{\partial^2 T_w}{\partial x^2} + \frac{\partial^2 T_w}{\partial y^2} + \frac{\partial^2 T_w}{\partial z^2} = 0 \tag{1}$$

Table 2
Thermophysical properties

	Material	ρ (kg/m^3)	λ (W/m K)	c_p (J/kg K)
Wall	Copper	8954	398	384
Particle	Bronze	8666	54	343
	Glass	2500	0.76	840
Fluid	Water	1000	0.6	4183

Table 1
Dimensions and porosities of the porous media

$d_p = 1.7$ mm			$d_p = 1.2$ mm			$d_p = 0.6$ mm		
a (mm)	ε_m	ε_w	a (mm)	ε_m	ε_w	a (mm)	ε_m	ε_w
1.68	0.458	0.973	1.18	0.450	0.965	0.59	0.450	0.965
1.64	0.420	0.934	1.16	0.423	0.937	0.58	0.423	0.937
1.75	0.520	1.0	1.25	0.537	1.0	0.65	0.588	1.0

Energy equation for the solid particles:

$$\frac{\partial^2 T_s}{\partial x^2}+\frac{\partial^2 T_s}{\partial y^2}+\frac{\partial^2 T_s}{\partial z^2}=0 \tag{2}$$

Mass, momentum and energy equations for the fluid:

$$\rho\left(\frac{\partial u}{\partial x}+\frac{\partial v}{\partial y}+\frac{\partial w}{\partial z}\right)=0 \tag{3}$$

$$\rho\left(u\frac{\partial u}{\partial x}+v\frac{\partial u}{\partial y}+w\frac{\partial u}{\partial z}\right)=-\frac{\partial p}{\partial x}+\mu\left(\frac{\partial^2 u}{\partial x^2}+\frac{\partial^2 u}{\partial y^2}+\frac{\partial^2 u}{\partial z^2}\right) \tag{4}$$

$$\rho\left(u\frac{\partial v}{\partial x}+v\frac{\partial v}{\partial y}+w\frac{\partial v}{\partial z}\right)=-\frac{\partial p}{\partial y}+\mu\left(\frac{\partial^2 v}{\partial x^2}+\frac{\partial^2 v}{\partial y^2}+\frac{\partial^2 v}{\partial z^2}\right) \tag{5}$$

$$\rho\left(u\frac{\partial w}{\partial x}+v\frac{\partial w}{\partial y}+w\frac{\partial w}{\partial z}\right)=-\frac{\partial p}{\partial z}+\mu\left(\frac{\partial^2 w}{\partial x^2}+\frac{\partial^2 w}{\partial y^2}+\frac{\partial^2 w}{\partial z^2}\right) \tag{6}$$

$$\rho c_p\left(u\frac{\partial T}{\partial x}+v\frac{\partial T}{\partial y}+w\frac{\partial T}{\partial z}\right)=\lambda\left(\frac{\partial^2 T}{\partial x^2}+\frac{\partial^2 T}{\partial y^2}+\frac{\partial^2 T}{\partial z^2}\right) \tag{7}$$

Fig. 2 shows the grid distribution in the porous media. The unstructured mesh used about 400,000 elements. Each particle had 400–800 nodes with 2000–4000 elements. The spaces between adjacent particles had about 500 nodes. Calculations with various numbers of elements showed that the results were grid independent. The convergence criteria required a decrease of at least 6 orders of magnitude for the residuals with no observable change in the surface temperatures for an additional 200 iterations.

The reliability of the calculations was verified in Jiang and Lu (2006) where the Reynolds numbers based on the particle diameters ($d_p = 1.7$, 1.2 and 0.6 mm) and the inlet velocity were 4.57–231, so the fluid flow in the porous media was in the laminar, transitional and turbulent flow regions. The k–ω turbulent model was used in the numerical calculations for the turbulent flow. The calculations for a porous medium of glass and water predicted an effective thermal conductivity for the porous media of 0.668 W/(m K) for $\varepsilon_m = 0.354$ which agreed well with the value from the well-known equations proposed by Zehener (1970) of $\lambda_m = 0.699$ W/(m K) for the same porosity of $\varepsilon_m = 0.354$. Comparisons of the predicted values of K and F from the numerical results and those calculated using well-known correlations (Ergun, 1952; Vafai, 1984, 1986) for the three particle diameters showed that the numerical results agree within 15% of the predictions except for a relatively large deviation in F for the 0.6 mm diameter particles. Jiang and Lu (2006) also compared the calculated local heat transfer coefficients for convection heat transfer of water in the sintered bronze porous plate channels with the experimental data of Jiang et al. (2004b) for 1.7, 1.2 and 0.6 mm diameter particles with three different velocities for each particle size. The numerical results agreed well with the experimental data, indicating that the particle-level direct numerical simulations can model the fluid flow and heat transfer in the complete porous media. The small deviations of the numerical results from the correlations and the experimental data may have been caused by differences between the mean porosities in the numerical model and in the experimental porous plate channel and by the non-uniform particle diameters, non-uniform porosities and random particle distributions in the experimental geometry.

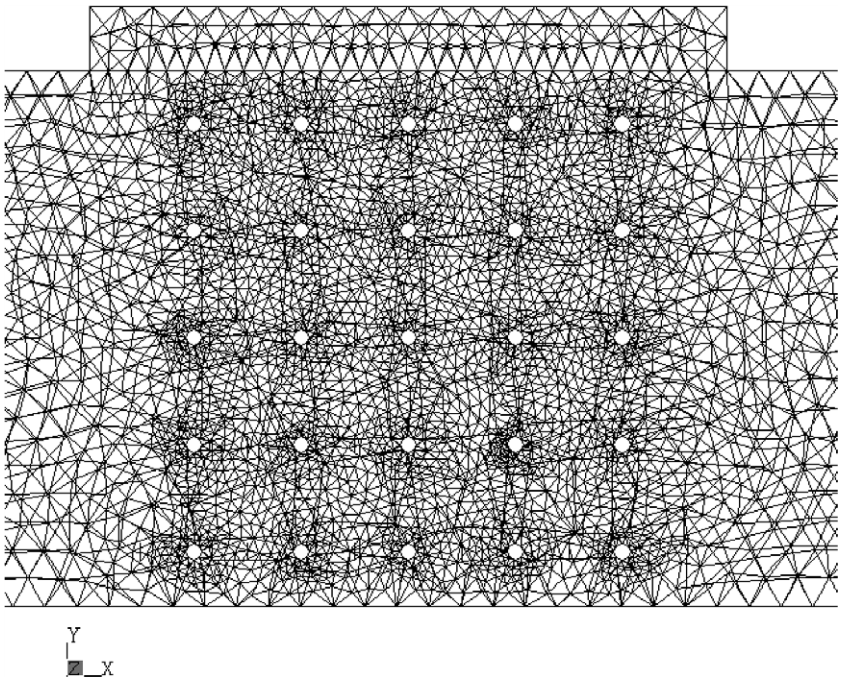

Fig. 2. Grid distribution in the porous media for $d_p = 1.7$ mm.

3. Numerical results and theoretical analysis

3.1. Temperature distributions in the porous media

The two-dimensional temperature distributions in the x–y-plane in the porous media with the zero and finite-thickness walls with and without thermal contact resistances are shown in Fig. 3. As mentioned above, the thermal contact resistance between particles and between the particles and the wall in non-sintered porous media was modeled using a 50 μm gap filled with water between the solid surfaces. The porous media temperature increases with increasing x and decreases with increasing distance from the contact interface. With the zero-thickness wall without thermal contact resistance between the particles, the solid particle temperature differs greatly from the adjacent fluid temperatures near the wall (Fig. 3a). Close to the contact surface between the wall and the upper row of solid particles, the solid particle temperatures are lower than the nearby fluid temperature. With the finite-thickness wall without thermal contact resistance, the wall temperature is quite uniform due to its high thermal conductivity (Fig. 3b). With the finite-thickness wall with thermal contact resistance (Fig. 3c), the wall temperature varies with the temperatures at the contact points with the solid particles being much lower than that of the areas in contact with the fluid. For this case, the heat is not easily transferred into the channel from the top surface, so the fluid temperatures in the channel are much lower than the particle temperatures.

Fig. 4 shows the two-dimensional temperature distribution at the wall–particle interface between the solid particles and the wall for the three sets of conditions. For the porous media with zero-thickness wall without thermal contact resistances, the solid temperature is much lower than the nearby fluid temperatures at the contact interface due to the large thermal conductivity differences between the fluid and the solid particles (Fig. 4a). The temperature increases along the fluid flow direction as the fluid temperature increases. For the porous media with the finite-thickness wall without thermal contact resistances, the temperature distribution is much more uniform although the fluid temperatures are still lower than the solid temperatures at adjacent locations (Fig. 4b). For the porous media with the finite-thickness heated wall with thermal contact resistances, the solid temperatures are also much lower than the nearby fluid temperatures at the contact interface, but the difference between the solid and fluid temperatures is less than for the zero-thickness wall due to heat conduction in the wall (Fig. 4c).

Fig. 5 shows the contact interface temperature distributions for the three conditions. Here, T_{w1} is the temperature on the wall–particle contact surface along a line parallel to the x-axis in the flow direction across the fluid and solid phase contact points at the interface (line 1 in Fig. 4), while T_{w2} is the wall surface temperature along a line between adjacent particles (line 2 in Fig. 4). T_f is the bulk fluid temperature. For the porous media with zero-thickness wall without thermal contact resistances, the fluid and solid temperatures at the contact interface differ greatly for this porous media with a large thermal conductivity difference between the fluid and the solid particles. For the porous media with finite-thickness heated wall without thermal contact resistances, the temperature distribution is much more uniform, while for the porous media with finite-thickness wall with thermal contact resistances, the solid temperature is again much less than the nearby fluid temperatures at the contact interface. The difference between the solid and fluid temperatures is less than the case with the zero-thickness wall due to heat conduction in the heated wall. Comparing the temperature distributions at the contact surface in the porous media for zero and finite-thickness walls without thermal contact resistances shows that the convection heat transfer coefficient with the finite-thickness wall is larger than with the zero-thickness wall. Therefore, the heated wall increases the fin effect in the porous media which intensifies the overall convection heat transfer. However, the thermal contact resistance between the particles and the wall reduces the overall convection heat transfer.

The temperature distributions show that the heat transfer coefficients in the porous media without thermal contact resistances are much larger than those in the porous media with thermal contact resistances which is consistent with the experimental results in Jiang et al. (2004b).

3.2. Heat flux distributions at the contact interface in the porous media

Fig. 6 shows the heat flux distributions at the wall–particle interface in the porous media with a finite wall thickness without thermal contact resistances for various porosities. The solid line is the heat flux distribution on the wall–particle contact surface along a line parallel to the x-axis across the fluid and solid phases at the interface (line 1 in Fig. 4), while the dotted line is the heat flux distribution on the wall surface along a line between adjacent particles (line 2 in Fig. 4). With a constant wall heat flux boundary condition on the top wall surface, the heat fluxes transferred into the fluid and the solid phases at adjacent locations on the contact interface are very different. The fluid and solid temperatures at adjacent locations are also not the same as shown in Fig. 5, but the temperature differences are much less than the heat flux differences at the contact interface shown in Fig. 6. The contact surface area between the particles and the wall is bigger in Fig. 6b than in Fig. 6a due to smaller porosity. As shown in Fig. 6a and b, the heat flux to the solid phase is much more than that to the fluid phase because of the large difference in the thermal conductivities. In Fig. 6a, the heat flux at the top wall surface is 1×10^5 W/m^2, while the maximum heat flux to the solid phase reaches 6.6×10^6 W/m^2 with the heat flux to the fluid phase of only about 1.6×10^4 W/m^2. Similarly, in Fig. 6b, the maximum heat flux to the solid phase reaches 2.2×10^6 W/m^2, while the heat flux to the fluid

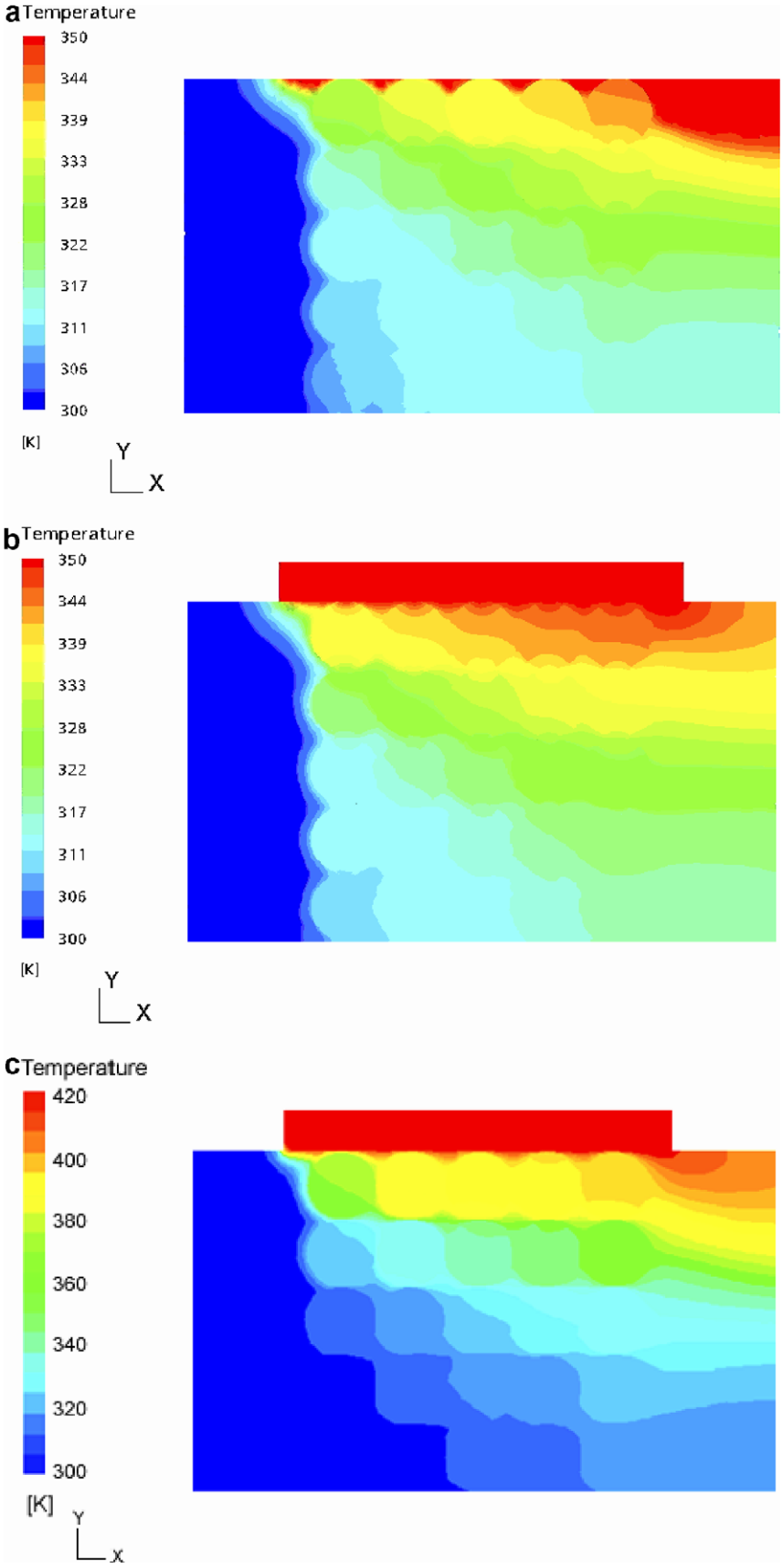

Fig. 3. Temperature distributions in the porous media with zero and finite-thickness heated walls with and without thermal contact resistances ($u_0 = 1$ mm/s, $q_{wo} = 1 \times 10^5$ W/m^2, $d_p = 1.7$ mm, $T_{f0} = 300$ K, $\varepsilon_m = 0.458$). (a) Zero-thickness wall without thermal contact resistances, (b) finite-thickness wall without thermal contact resistances, (c) finite-thickness wall with thermal contact resistances.

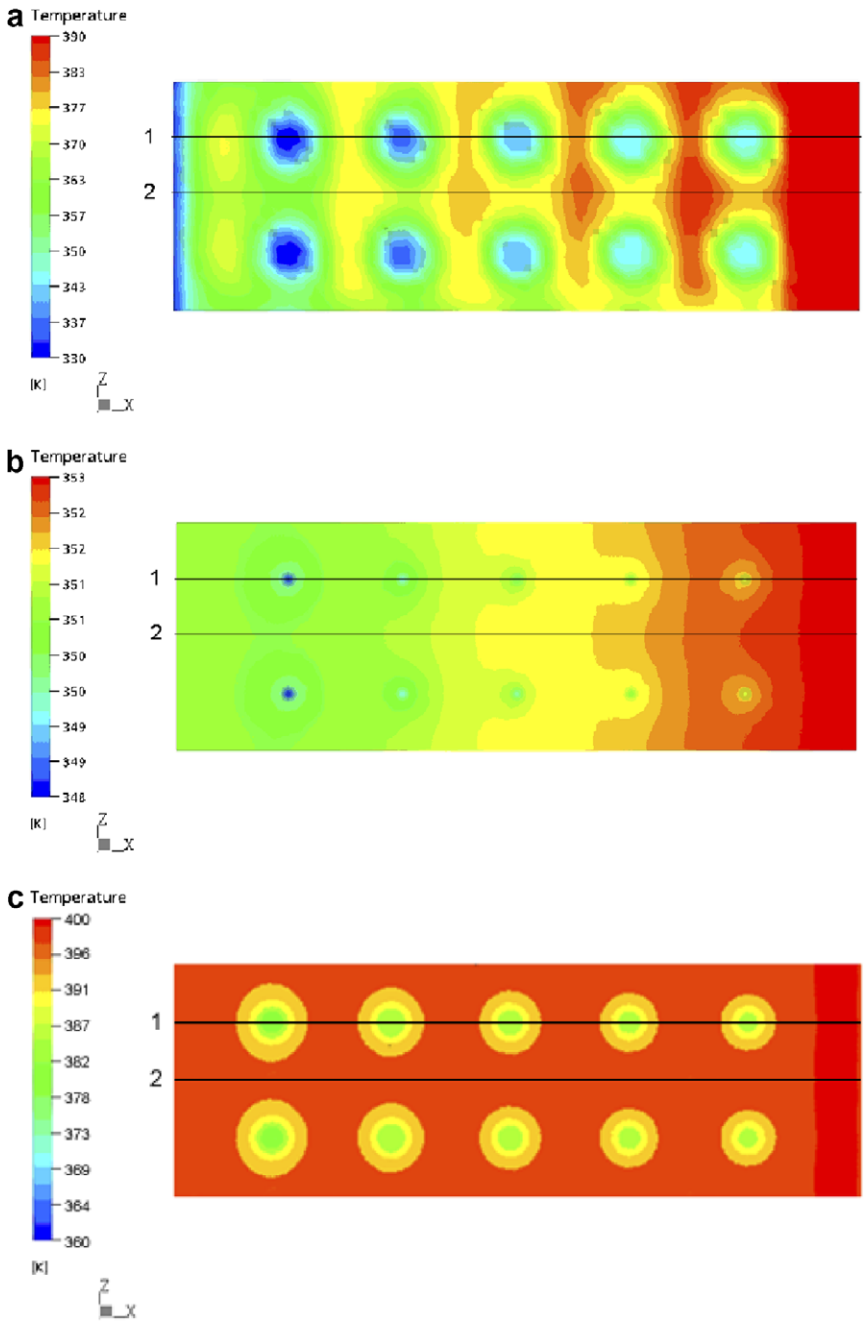

Fig. 4. Temperature distributions at the wall–particles interface with zero and finite-thickness heated walls with and without thermal contact resistances ($u_0 = 1$ mm/s, $q_{wo} = 1 \times 10^5$ W/m^2, $d_p = 1.7$ mm, $T_{f0} = 300$ K, $\varepsilon_m = 0.458$). (a) Zero-thickness wall without thermal contact resistances, (b) finite-thickness wall without thermal contact resistances, (c) finite-thickness wall with thermal contact resistances.

phase is only about 1.3×10^4 W/m^2. Therefore, the maximum heat flux to the solid phase increases with increasing porosity; although, the total heat transferred through the solid phase increases with decreasing porosity due to the larger contact surface area.

Fig. 7 shows the heat flux distributions at the wall–particle interface with a finite wall thickness with thermal contact resistances for the constant wall heat flux boundary conditions on the top wall surface. The heat fluxes transferred by the fluid and the solid at adjacent locations on the contact interface are very similar for this case with the heat flux differences being much less than for the case without thermal contact resistances.

3.3. Boundary conditions for the energy equations in porous media

These results have shown that the thermal contact resistance at the wall between the solid particles and the wall significantly affect the heat fluxes through the solid parti-

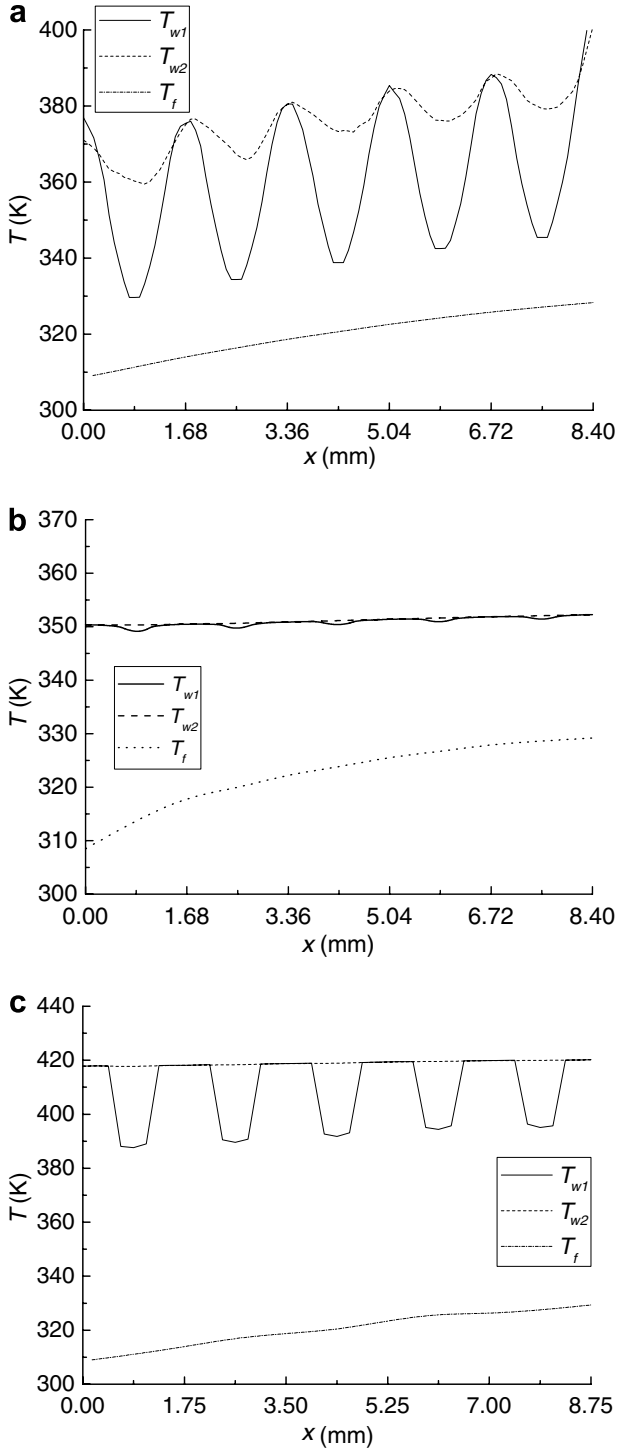

Fig. 5. Temperature distributions at the wall–particle interface with zero and finite-thickness heated walls with and without thermal contact resistances ($u_0 = 1$ mm/s, $q_{wo} = 1 \times 10^5$ W/m^2, $d_p = 1.7$ mm, $T_{f0} = 300$ K, $\varepsilon_m = 0.458$). (a) Zero-thickness wall without thermal contact resistances, (b) finite-thickness wall without thermal contact resistances, (c) finite-thickness wall with thermal contact resistances.

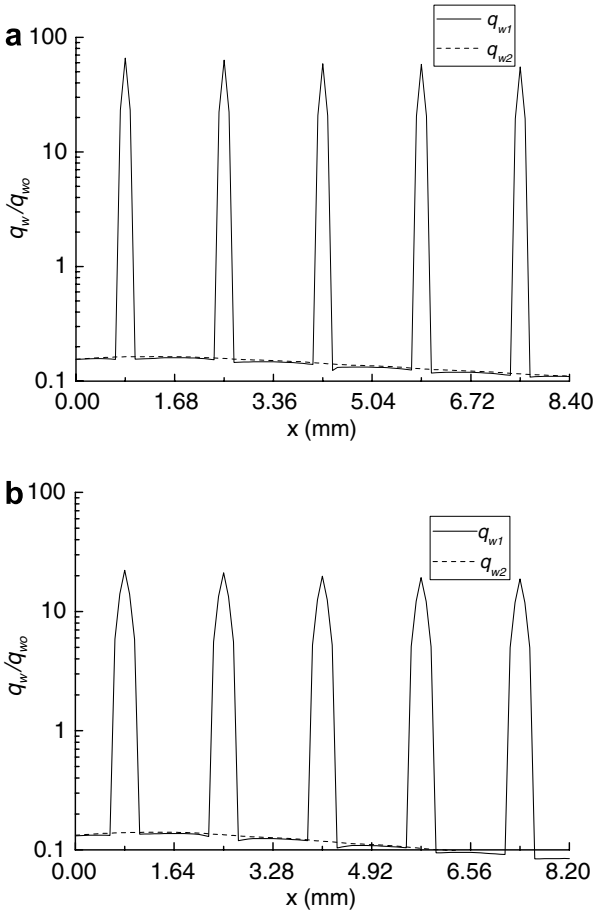

Fig. 6. Heat flux distributions at the wall–particle interface in the porous media with a finite-thickness wall without thermal contact resistances for various porosities ($u_0 = 1$ mm/s, $q_{wo} = 1 \times 10^5$ W/m^2, $d_p = 1.7$ mm, $T_{f0} = 300$ K). (a) $\varepsilon_m = 0.458$, (b) $\varepsilon_m = 0.420$.

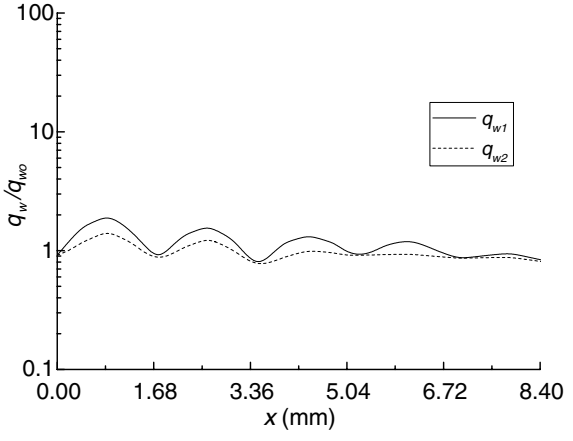

Fig. 7. Heat flux distribution at the wall–particle interface with a finite-thickness wall with thermal contact resistances ($u_0 = 1$ mm/s, $q_{wo} = 1 \times 10^5$ W/m^2, $d_p = 1.7$ mm, $T_{f0} = 300$ K, $\varepsilon_m = 0.458$).

cles and the fluid near the wall. Without the thermal contact resistance, the temperatures of the solid particles and the fluid near the wall are quite similar, while the heat fluxes are quite different. However, when the thermal contact resistance at the wall between the solid particles and the wall is considered, the particle temperatures at the contact surface are quite different from the fluid temperatures in the pores near the wall, while the heat fluxes

Table 3
Comparison of the thermal boundary characteristics for different cases in a porous media of bronze and water: $\lambda_s/\lambda_f = 54/0.6 = 90$

d_p (mm)	ε_m	ε_w	$\left(\frac{\bar{q}_s}{q_{wo}}\right)_N$	$\left(\frac{\bar{q}_f}{q_{wo}}\right)_N$	$\left(\frac{\bar{q}_s}{q_{wo}}\right)_C$	$\left(\frac{\bar{q}_f}{q_{wo}}\right)_C$	$\frac{-\lambda_m\left(\frac{\partial T}{\partial y}\right)_{f,w,N}}{q_{wo}}$	$\frac{q_{w,N}}{q_{wo}}$
1.7	0.458	0.973	34.3	0.14	26.4	0.294	1.03	1.06
1.7	0.420	0.934	11.3	0.11	13.1	0.145	0.892	0.849
1.2	0.450	0.965	25.8	0.13	21.9	0.243	0.982	1.03
1.2	0.423	0.937	12.8	0.12	13.6	0.151	0.965	0.919
0.6	0.450	0.965	30.9	0.14	21.9	0.243	1.07	1.22
0.6	0.423	0.937	15.3	0.13	13.6	0.151	1.05	1.09
1.7^C	0.520	0.973	1.40	0.98				

Note: superscript "C" indicates the case with thermal contact resistance.

$$q_{w,N} = -\varepsilon_w\lambda_f\left(\frac{\partial T_f}{\partial y}\right)_{w,N} - (1-\varepsilon_w)\lambda_s\left(\frac{\partial T_s}{\partial y}\right)_{w,N}.$$

Table 4
Comparison of the thermal boundary characteristics for different cases in a porous media of glass and water: $\lambda_s/\lambda_f = 0.76/0.6 = 1.27$

d_p (mm)	ε_m	ε_w	$\left(\frac{\bar{q}_s}{q_{wo}}\right)_N$	$\left(\frac{\bar{q}_f}{q_{wo}}\right)_N$	$\left(\frac{\bar{q}_s}{q_{wo}}\right)_C$	$\left(\frac{\bar{q}_f}{q_{wo}}\right)_C$	$\frac{-\lambda_m\left(\frac{\partial T}{\partial y}\right)_{f,w,N}}{q_{wo}}$	$\frac{q_{w,N}}{q_{wo}}$
1.7	0.458	0.973	11.5	0.70	1.26	0.993	1.05	0.992
1.7	0.420	0.934	4.71	0.62	1.24	0.983	0.945	0.890
1.2	0.450	0.965	9.90	0.66	1.25	0.991	1.04	0.983
1.2	0.423	0.937	5.51	0.60	1.25	0.983	0.958	0.909
0.6	0.450	0.965	12.9	0.63	1.25	0.991	1.10	1.06
0.6	0.423	0.937	7.19	0.58	1.25	0.983	1.03	0.996
1.7^C	0.458	0.973	1.02	1.00				

Note: superscript "C" indicates the case with thermal contact resistance.

$$q_{w,N} = -\varepsilon_w\lambda_f\left(\frac{\partial T_f}{\partial y}\right)_{w,N} - (1-\varepsilon_w)\lambda_s\left(\frac{\partial T_s}{\partial y}\right)_{w,N}.$$

through the particles and through the fluid are quite similar. Tables 3 and 4 present the calculated heat fluxes at the wall–particle interface (bronze and glass).

As mentioned in the Introduction, various methods to treat the energy equation boundary conditions can be used for the constant heat flux boundary condition on the outer surface of porous channels. The main differences are whether the fluid temperature is equal to the solid phase temperature at the boundary surface and how to determine the heat flux transferred through the solid phase and the fluid. Alazmi and Vafai (2002) analyzed 8 different forms of constant wall heat flux boundary conditions. They found that different boundary conditions may lead to substantially different results and selecting one model over the others is not an easy issue. Analysis of the different forms of the constant wall heat flux boundary conditions showed that the following most accurately represents the actual conditions.

$$q_w = \varepsilon q_f + (1-\varepsilon)q_s; \quad \frac{q_f}{q_s} = \frac{\lambda_f}{\lambda_s} \tag{8}$$

These can be rearranged to give:

$$q_s = \frac{\lambda_s}{\varepsilon\lambda_f + (1-\varepsilon)\lambda_s}q_w; \quad q_f = \frac{\lambda_f}{\varepsilon\lambda_f + (1-\varepsilon)\lambda_s}q_w \tag{9}$$

Tables 3 and 4 also compare the wall heat fluxes between the solid particles and the wall calculated using Eq. (9). If the thermal contact resistance is not considered (as in sintered porous media) for the porous media of bronze and water, the results calculated using Eq. (9) are similar to the numerical results, while for the porous media made of glass and water, the results calculated using Eq. (9) are very different from the numerical results. Therefore, the model for the thermal boundary conditions, Eq. (9), is not universal. When thermal contact resistances are included (as in non-sintered porous media), the heat fluxes transferred by the fluid and the solid phases are very close.

Fig. 8 presents the average wall temperatures of the parts contacting the fluid (T_{wf}) and the solid particles (T_{ws}), the average wall temperatures at the wall–particle interface (T_w), temperatures inside the wall (0.5 mm from the top surface, T_{wp}, which corresponds with the thermocouples in the experiments) and the fluid temperature (T_f) in the porous media for a finite wall thickness with and without thermal contact resistance. Without the thermal contact resistances (Fig. 8a), the average wall temperatures of locations in contact with the fluid (T_{wf}) and the solid particles (T_{ws}), and the average wall temperature at the

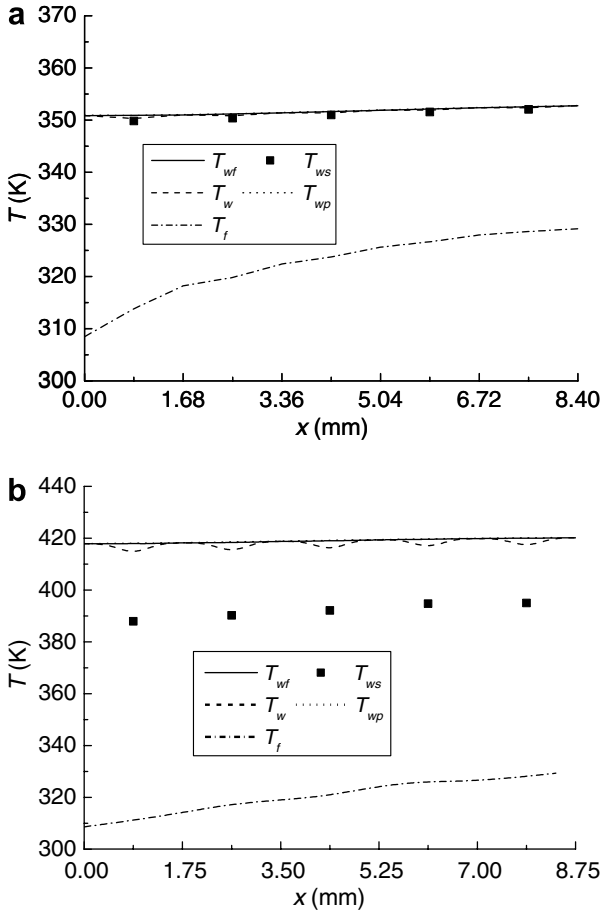

Fig. 8. Average wall temperatures on the wall surface and the fluid temperature in the porous media with a finite wall thickness with and without thermal contact resistances ($u_0 = 1$ mm/s, $q_{wo} = 1 \times 10^5$ W/m^2, $d_p = 1.7$ mm, $T_{f0} = 300$ K, $\varepsilon_m = 0.458$). (a) Finite-thickness wall without thermal contact resistances, (b) finite-thickness wall with thermal contact resistances.

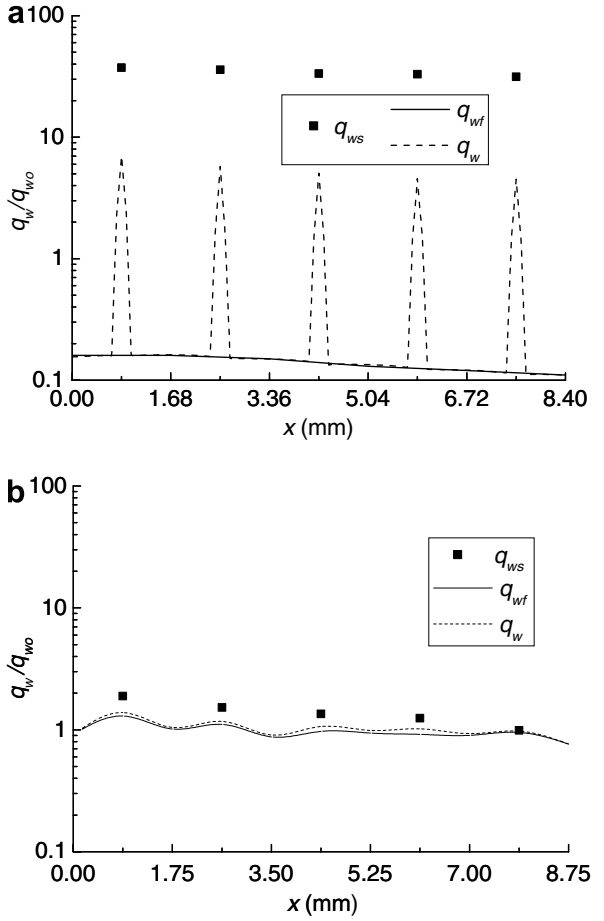

Fig. 9. Average heat flux distributions on the wall surface in the porous media with a finite wall thickness with and without thermal contact resistances ($u_0 = 1$ mm/s, $q_{wo} = 1 \times 10^5$ W/m^2, $d_p = 1.7$ mm, $T_{f0} = 300$ K, $\varepsilon_m = 0.458$). (a) Finite-thickness wall without thermal contact resistances, (b) finite-thickness wall with thermal contact resistances.

contact interface (T_w) are very similar. However, with the thermal contact resistances between the particles and on the wall (Fig. 8b), the average temperatures T_{wf}, T_{ws} and T_w are quite different.

Fig. 9 shows the average heat flux distributions on the wall of locations in contact with the fluid (q_{wf}) and the solid particles (q_{ws}), and the overall average heat flux distribution on the surface (q_w) in the porous media with a finite wall thickness with and without thermal contact resistances. Without thermal contact resistances (Fig. 9a), the average heat fluxes through the solid phase (q_{ws}) and fluid (q_{wf}) at the contact interface are very different, with a non-uniform overall average heat flux at the wall surface (q_w). With thermal contact resistances between the particles and on the wall surface (Fig. 9b), the average heat fluxes of the solid phase (q_{ws}) and fluid (q_{wf}) at the contact interface are very similar. The general average heat fluxes of the solid phase (q_{ws}) and the fluid (q_{wf}) at the wall surface are fairly similar to the heat flux on the outer surface, and the overall average heat flux at the contact interface (q_w) is quite uniform.

As shown by Jiang (2001, 2004a), there are primarily four methods for treating the constant wall heat flux boundary conditions for the energy equations:

Amiri et al. (1995) and Jiang et al. (1996, 1999):

$$q_w = -\lambda_{fw}(\partial T_f/\partial y)_w = -\lambda_s(\partial T_f/\partial y)_w \tag{10}$$

Martin et al. (1998):

$$q_w = -(\varepsilon\lambda_f + (1-\varepsilon)\lambda_s)_w(\partial T/\partial y)_w; \quad T_{ws} = T_{wf} \tag{11}$$

Lee and Vafai (1999):

$$q_w = -\varepsilon_w\lambda_{fw}(\partial T_f/\partial y)_w - (1-\varepsilon_w)\lambda_s(\partial T_s/\partial y)_w; \quad T_{ws} = T_{wf} \tag{12}$$

Jiang et al. (2004a):

$$q_w = -\lambda_m(\partial T/\partial y)_w; \quad T_{ws} = T_{wf} \tag{13}$$

Where the effective thermal conductivity of the porous media can be calculated from the well-known equations proposed by Zehener (1970):

$$\frac{\lambda_m}{\lambda_f} = [1-\sqrt{1-\varepsilon}] + \frac{2\sqrt{1-\varepsilon}}{1-\sigma B}\left[\frac{(1-\sigma)B}{(1-\sigma B)^2}\ln\left(\frac{1}{\sigma B}\right) - \frac{B+1}{2} - \frac{B-1}{1-\sigma B}\right] \quad (14)$$

where,

$$B = 1.25((1-\varepsilon)/\varepsilon)^{10/9}; \quad \sigma = \lambda_f/\lambda_s$$

Previous analyses by Jiang and Ren (2001) and Jiang et al. (2002, 2004a) showed that numerical simulations of convection heat transfer of air and water in non-sintered packed beds using a local thermal non-equilibrium model with the assumption that the heat fluxes into the solid and the fluid from the heat transfer surface were the same (as Eq. (10)) with a variable porosity model agreed well with the experimental data. For numerical simulations of convection heat transfer in sintered porous media, the boundary conditions on the wall should be that the particle temperatures are equal to the fluid temperatures (as in Eqs. (11)–(13)). Jiang et al. (2004a) showed that Eq. (13) gave satisfactory results that compared well with experimental data for sintered porous media.

Tables 3 and 4 list the calculated results for $-\lambda_m(\partial T/\partial y)_{f,w,N}/q_{w0}$ where λ_m was calculated using Eq. (14) with the mean porosity ε_m. The values are quite close to 1 for both types of the porous media with bronze and glass particles. Tables 3 and 4 also list the calculated results for $\left(-\varepsilon_w\lambda_f\left(\frac{\partial T_f}{\partial y}\right)_{w,N} - (1-\varepsilon_w)\lambda_s\left(\frac{\partial T_s}{\partial y}\right)_{w,N}\right)\Big/q_{w0}$. From the physical meaning, the value of $\left(-\varepsilon_w\lambda_f\left(\frac{\partial T_f}{\partial y}\right)_{w,N} - (1-\varepsilon_w)\lambda_s\left(\frac{\partial T_s}{\partial y}\right)_{w,N}\right)\Big/q_{w0}$ should be exactly equal to 1, so the departure from 1 most likely indicates numerical errors.

Therefore, the results indicate that the distribution of the heat fluxes between the solid phase and the fluid at the contact interface without thermal contact resistance is related to the ratio of the thermal conductivities of the solid and the fluid, the ratio of the thermal conductivities of the plate and the solid particles, the ratio of the wall thickness to the particle diameter, the ratio of the wall porosity to the mean porosity and the Biot number. Therefore, the proper model for the constant wall heat flux boundary conditions in porous media with a finite wall thickness without thermal contact resistance is

$$q_w = \varepsilon q_f + (1-\varepsilon)q_s \quad (15)$$

$$\frac{q_s}{q_f} = f(\lambda_s/\lambda_f, \lambda_w/\lambda_s, \varepsilon_w/\varepsilon_m, \delta/d_p, h\delta/k_w) \quad (16)$$

However, this is very complicated. From the abovementioned results the following models should be a good approximation for the constant wall heat flux boundary conditions in porous media with a finite wall thickness without thermal contact resistance (as in sintered porous media):

$$q_w = -\varepsilon_w\lambda_{fw}(\partial T_f/\partial y)_w - (1-\varepsilon_w)\lambda_s(\partial T_s/\partial y)_w; \quad T_{ws} = T_{wf} \quad (17)$$

or

$$q_w = -\lambda_m(\partial T/\partial y)_w; \quad T_{ws} = T_{wf} \quad (18)$$

For convection heat transfer in porous media with a finite wall thickness with thermal contact resistances (as in non-sintered porous media), the numerical simulations in the present research and previous experimental and numerical investigations in Jiang and Ren (2001) and Jiang et al. (1996, 2002) suggest that the thermal boundary conditions for the constant wall heat flux boundary condition on the outer surface should be

$$q_w \approx q_f \approx q_s \quad (19)$$

4. Conclusions

(1) For porous media with a zero-thickness heated wall, the fluid and solid temperatures at the wall surface depend strongly on the thermal conductivity ratio between the fluid and solid particles. For porous media with a finite-thickness heated wall without thermal contact resistances, the temperature distribution between the solid and fluid near the wall is quite uniform, while for porous media with a finite-thickness heated wall with thermal contact resistances, the solid temperature is much lower than the nearby fluid temperature near the wall surface.

(2) For the constant wall heat flux boundary conditions on the top wall surface without thermal contact resistance, the heat fluxes into the fluid and the solid phases at adjacent locations on the contact interface are quite different. The maximum heat flux to the solid increases with increasing porosity, while the total heat transferred by the solid increases with decreasing porosity due to the larger contact surface area with the smaller porosities. However, the heat flux distributions at the wall surface in the porous media with a finite wall thickness with thermal contact resistances are quite uniform.

(3) A good approximation for the constant wall heat flux boundary condition for convection heat transfer in porous media with a finite wall thickness without thermal contact resistance (as in sintered porous media) is $T_{ws} \approx T_{wf}$, while the proper model for the constant wall heat flux boundary condition for convection heat transfer in porous media with a finite wall thickness with thermal contact resistances (as in non-sintered porous media) is $q_w \approx q_f \approx q_s$.

Acknowledgement

The project was supported by the National Outstanding Youth Fund from the National Natural Science Foundation of China (No. 50025617). We thank Prof. David Christopher for editing the English.

References

Alazmi, B., Vafai, K., 2002. Constant wall heat flux boundary conditions in porous media under local thermal non-equilibrium conditions. Int. J. Heat Mass Transfer 45, 3071–3087.

Amiri, A., Vafai, K., 1994. Analysis of dispersion effects and non-thermal equilibrium, non-Darcian, variable porosity incompressible flow through porous media. Int. J. Heat Mass Transfer 37 (6), 939–954.

Amiri, A., Vafai, K., Kuzay, T.M., 1995. Effects of boundary conditions on non-Darcian heat transfer through porous media and experimental comparisons. Numer. Heat Transfer, Part A 27, 651–664.

Çengel, Y.A., Turner, R.H., 2001. Fundamentals of Thermal–Fluid Sciences. McGraw-Hill International Edition.

Ergun, S., 1952. Fluid flow through packed columns. Chem. Eng. Process. 48, 89–94.

Hsieh, W.H., Lu, S.F., 2000. Heat-transfer analysis and thermal dispersion in thermally-developing region of a sintered porous metal channel. Int. J. Heat Mass Transfer 43, 3001–3011.

Incropera, F.P., DeWitt, D.P., 1996. Fundamentals of Heat and Mass Transfer, fourth ed. John Wiley & Sons.

Jiang, P.X., 2001. Analysis of the thermal characteristics on the boundary in porous media. In: Proc. National Heat and Mass Transfer Conference, Qingdao, Shandong, pp. 514–518 (in Chinese).

Jiang, P.X., Lu, X.C., 2006. Numerical simulation of fluid flow and convection heat transfer in sintered porous plate channels. Int. J. Heat Mass Transfer 49 (9–10), 1685–1695.

Jiang, P.X., Ren, Z.P., 2001. Numerical investigation of forced convection heat transfer in porous media using a thermal non-equilibrium model. Int. J. Heat Fluid Flow 22 (1), 102–110.

Jiang, P.X., Ren, Z.P., Wang, B.X., Wang, Z., 1996. Forced convective heat transfer in a plate channel filled with solid particles. J. Therm. Sci. 5, 43–53.

Jiang, P.X., Ren, Z.P., Wang, B.X., 1999. Numerical simulation of forced convection heat transfer in porous plate channels using thermal equilibrium or non-thermal equilibrium models. Numer. Heat Transfer 35 (Part A), 99–113.

Jiang, P.X., Li, M., Ren, Z.P., 2002. Forced convection heat transfer in plate channels filled with packed beds or sintered porous media. Tsinghua Sci. Technol. 7 (2), 202–208.

Jiang, P.X., Li, M., Ma, Y.C., Ren, Z.P., 2004a. Boundary conditions and wall effect for forced convection heat transfer in sintered porous plate channels. Int. J. Heat Mass Transfer 47 (10–11), 2073–2083.

Jiang, P.X., Li, M., Lu, T.J., Yu, L., Ren, Z.P., 2004b. Experimental research on convection heat transfer in sintered porous plate channels. Int. J. Heat Mass Transfer 47 (10–11), 2085–2096.

Kim, S.J., Kim, D., 2001. Thermal interaction at the interface between a porous medium and an impermeable wall. J. Heat Transfer 123 (3), 527–533.

Lee, D.Y., Vafai, K., 1999. Analytical characterization and conceptual assessment of solid and fluid temperature differences in porous media. Int. J. Heat Mass Transfer 42, 423–435.

Martin, A.R., Saltiel, C., Shyy, W., 1998. Heat transfer enhancement with porous inserts in recirculating flows. J. Heat Transfer 120, 458–467.

Peterson, G.P., Chang, C.S., 1998. Two-phase heat dissipation utilizing porous-channels of high-conductivity materials. J. Heat Transfer 120, 243–252.

Quintard, M., 1998. Modelling local non-equilibrium heat transfer in porous media, Heat Transfer 1998. In: Proc. 11th Int. Heat Transfer Conference, Kyongju, Korea, vol. 1, pp. 279–285.

Vafai, K., 1984. Convective flow and heat transfer in variable-porosity media. J. Fluid Mech. 147, 233–259.

Vafai, K., 1986. Analysis of the channeling effect in variable porosity media. J. Energy Resour. Technol. 108, 131–139.

Zehener, P., 1970. Waermeleitfahigkeit won Schuettungen be Massigen Temperaturea. Chem.-Ingr.-Tech. 42, 933–941.